

Energy transfer from a semiconductor quantum dot to an organic matrix

D.M. Basko¹, V.M. Agranovich², F. Bassani¹, and G.C. La Rocca^{1,3,a}

¹ INFN and Scuola Normale Superiore, Piazza dei Cavalieri, 56126 Pisa, Italy

² Institute of Spectroscopy, Russian Academy of Sciences, 142092, Troitsk, Moscow Region, Russia

³ Dipartimento di Fisica, Università di Salerno, via S. Allende, 84081 Baronissi (Sa), Italy

Received 2 July 1999

Abstract. Förster energy transfer from an excited semiconductor quantum dot to the surrounding organic material is considered. While earlier only the calculations for the lowest excited state of the dot were performed and only the limiting cases of strong and weak confinement were analyzed, in this work we present the results for the crossover region, obtained from the variational calculation. We also consider the transfer from the higher excited states, which may be relevant if the carrier relaxation in the dot is inhibited due to the discreteness of the states. We employ a microscopic quantum mechanical description of the Wannier-Mott exciton in the quantum dot and a macroscopic description of the organic medium. According to our calculations, for II-VI type semiconductors (like CdSe) and strongly absorbing organics (like PTCDA) the energy transfer may occur on time scales of several tens of picoseconds, which is significantly less than the quantum dot excitation lifetime in the absence of such transfer. Thus, as in the case of quantum wells, the Förster mechanism may be an efficient tool for pumping organic light-emitting substances. In this paper we also consider how the carrier intraband relaxation time in the dot may be affected by the Förster energy transfer.

PACS. 78.66.-w Optical properties of specific thin films, surfaces, and low-dimensional structures – 78.20.Bh Theory, models, and numerical simulation – 78.66.Qn Polymers; organic compounds

1 Introduction

Hybrid nanostructures based on semiconductor and organic materials with close exciton energies [1] were considered theoretically in different configurations and were shown to have certain advantages in comparison to traditional nanostructures, purely organic or purely inorganic [1–6]. These configurations can be divided into two groups. In the first case (strong coupling regime) the characteristic energy of the dipole-dipole interaction of Wannier-Mott excitons (in the semiconductor) and Frenkel excitons (in the organics) is larger than their level widths. As a result, new elementary excitations appear, being the coherent superposition of the two types of excitons [1–3, 6]. Such systems were shown to have enhanced optical nonlinearities.

In the second case (weak coupling regime) the level width is larger than the resonant interaction energy. In such situation, which is common for many organic substances, dephasing processes destroy the coherent superposition of excitonic states. Instead, incoherent energy transfer from the subsystem with the weaker dissipation (donor) to the subsystem where dissipative processes are stronger (acceptor), takes place. This corresponds to the

Förster picture of energy transfer [7]. The most relevant case is when the semiconductor part of the structure plays the role of the donor, and the organic part – of the acceptor. If the characteristic transfer time is less than or comparable to the Wannier-Mott exciton lifetime, then a significant fraction of the excitation energy can be transferred from the semiconductor to the organics. This gives the possibility to combine comparatively good transport properties of semiconductors (*e.g.*, pumped electrically [8, 9]) and good light-emitting properties of organic substances. Calculations performed for the planar geometry (semiconductor quantum well, covered by an organic overlayer) [4, 5], have shown that such transfer indeed may be quite efficient.

One family of semiconductor nanostructures, widely studied in recent years, is that of quantum dots (see [10] and references therein). Förster energy transfer from a semiconductor quantum dot to the surrounding organic medium has also been predicted [11]. In reference [11] only the transfer rate from the lowest excited state of the dot was calculated and only the limiting cases of strong and weak confinement (in other words, the dot size much smaller or much larger than the exciton Bohr radius) were considered. However (see Ref. [12] and references therein), due to the discreteness of states, carrier relaxation in

^a e-mail: larocca@ella.sns.it

quantum dots happens in a way qualitatively different from that in higher-dimensionality nanostructures. The role and efficiency of different relaxation mechanisms is not yet clear [10,12], so we consider the problem of the energy transfer from higher levels of the dot to be relevant. We also show that the carrier relaxation itself may be affected by Förster transfer.

In the present paper we (i) look at the transfer rate from the higher excited states, and (ii) present the results for intermediate dot sizes obtained from a variational calculation. For simplicity we consider a spherical quantum dot and describe the Wannier-Mott exciton in the effective mass approximation. Such description (as well as the use of the semiconductor background dielectric constant to describe the screening) implies that the size of the dot should be significantly larger than the lattice constant. For the organic subsystem the macroscopic description employing the complex dielectric function is satisfactory [5], since the length scale of field variation in the organics is much larger than the molecular length scale. In Section 2 we describe the general scheme of the Förster energy transfer rate calculation for a hybrid nanostructure, in Section 3 we derive general relations for the spherical geometry, Section 4 describes the results for different excited states in the limiting cases of strong and weak confinement, in Section 5 we compare these results with those obtained from simple variational calculation for the lowest excited state.

As for the possible experimental configurations where the predicted effects could be observed, the continuous technological progress in the growth and characterization of quantum dots such as overgrown self-organized dots or stabilized nanocrystal colloids is very promising; however, a detailed analysis of specific material systems is beyond the scope of the present paper.

2 The transfer rate

We consider a nanostructure consisting of a spherical quantum dot of radius R with dielectric constant ε , surrounded by a concentric semiconductor barrier with thickness L_b and the same dielectric constant. The barrier is assumed to be infinitely high, thus carriers cannot penetrate it. The space outside the barrier is filled with the organic substance with dielectric constant $\tilde{\varepsilon}$. The quantity ε includes only the contribution of higher resonances (with respect to the exciton resonance under consideration) and we consider it to be real. The quantity $\tilde{\varepsilon}$ is the total dielectric constant of the organic material and is complex in the frequency range of interest, which corresponds to absorption.

Here we use the same scheme of the Förster energy transfer rate calculation for a hybrid nanostructure, as employed in references [4,5,11], and discussed in detail in reference [5]. This approach [13] is equivalent to the usual Förster theory within the appropriate conditions for its applicability (in particular, the energy back transfer should be negligible) as discussed in reference [7]. In the case considered here the transfer rate may be found from

the calculation of the Joule losses of the electric field produced in the organic medium by the exciton polarization of the quantum dot.

Let the electron-hole pair in the dot be described by the envelope wave function $\psi(\mathbf{r}_e, \mathbf{r}_h)$ with the corresponding energy $\hbar\omega$ ($\mathbf{r}_e, \mathbf{r}_h$ being the electron and hole coordinates). Let also \mathbf{d}^{vc} be the matrix element of the electric dipole moment between the Bloch functions of the conduction and valence band extrema. Following the approach of reference [5], the exciton polarization in the quantum dot is written as

$$\mathbf{P}(\mathbf{r}) = \mathbf{d}^{\text{vc}} \psi(\mathbf{r}, \mathbf{r}). \quad (1)$$

The electric field $\mathcal{E}(\mathbf{r})$ corresponding to this polarization may be found from the Poisson equation for the potential $\phi(\mathbf{r})$:

$$\varepsilon(r) \nabla^2 \phi(\mathbf{r}) = 4\pi \operatorname{div} \mathbf{P}(\mathbf{r}), \quad (2)$$

where $\varepsilon(r) = \varepsilon$ at $r < R + L_b$ and $\varepsilon(r) = \tilde{\varepsilon}$ at $r > R + L_b$, with the corresponding boundary conditions at $r = R + L_b$. Knowing the electric field, we can calculate the power dissipated in the organic medium (Joule losses) [14] (the application of this semiclassical approach to quantum transitions was explained in detail in Ref. [5]):

$$W = \frac{\omega \operatorname{Im} \tilde{\varepsilon}(\omega)}{2\pi} \int_{r>R+L_b} |\mathcal{E}(\mathbf{r})|^2 d^3\mathbf{r}. \quad (3)$$

From here we find that the transfer rate (inverse transfer time) is given by

$$\frac{1}{\tau} = \frac{W}{\hbar\omega} = \frac{\operatorname{Im} \tilde{\varepsilon}(\omega)}{2\pi\hbar} \int_{r>R+L_b} |\mathcal{E}(\mathbf{r})|^2 d^3\mathbf{r}. \quad (4)$$

3 The electric field in the organics

In the spherical geometry the states of the electron-hole pair may be classified by the total angular momentum quantum numbers l, m , which determines the angular dependence of the electron-hole pair wave function

$$\psi(\mathbf{r}, \mathbf{r}) \propto Y_{lm}(\theta, \varphi), \quad (5)$$

where $Y_{lm}(\theta, \varphi)$ are the spherical harmonic functions. The case of the lowest excited state, considered in reference [11] corresponds to $l = m = 0$. Putting the z axis along the vector \mathbf{d}^{vc} , for the polarization we may write

$$P_z(\mathbf{r}) = P^{(r)}(r) Y_{lm}(\theta, \varphi), \quad (6)$$

which corresponds to the charge density:

$$\begin{aligned} \rho(\mathbf{r}) &= -\operatorname{div} \mathbf{P}(r) = -\frac{\partial P}{\partial z} \\ &= \rho_{l-1}^{(r)}(r) Y_{l-1,m} + \rho_{l+1}^{(r)}(r) Y_{l+1,m}. \end{aligned} \quad (7)$$

After some algebra the functions $\rho_{l\mp 1}^{(r)}(r)$ defined by the preceding equation may be related to $P^{(r)}(r)$:

$$i\rho_{l-1}^{(r)}(r) = \sqrt{\frac{l^2 - m^2}{4l^2 - 1}} \left[\frac{dP^{(r)}}{dr} + (l+1) \frac{P^{(r)}}{r} \right], \quad (8)$$

$$i\rho_{l+1}^{(r)}(r) = \sqrt{\frac{(l+1)^2 - m^2}{4(l+1)^2 - 1}} \left[-\frac{dP^{(r)}}{dr} + l \frac{P^{(r)}}{r} \right]. \quad (9)$$

The electrostatic potential $\phi(\mathbf{r})$, satisfying the Poisson equation (2), may be also decomposed analogously to the equation (7). The terms with $Y_{l-1,m}$ and $Y_{l+1,m}$ separate in the Poisson equation and we have two equations for the radial parts of the potential $\phi_\lambda^{(r)}(r)$ with $\lambda = l-1, l+1$:

$$\frac{1}{r^2} \frac{d}{dr} \left(r^2 \frac{d\phi_\lambda^{(r)}}{dr} \right) - \frac{\lambda(\lambda+1)}{r^2} \phi_\lambda^{(r)} = -4\pi \rho_\lambda^{(r)}(r), \quad (10)$$

where $\rho_\lambda^{(r)}(r)$ vanishes at $r > R$ (as $P(r)$ does). A general solution in a region, free of charges, corresponds to the 2^λ -pole potential [15]:

$$\phi_\lambda^{(r)}(R < r < R + L_b) = \sqrt{\frac{4\pi}{2\lambda+1}} \times \left[\frac{Q_\lambda^{\text{exc}}}{\varepsilon r^{\lambda+1}} + Q_\lambda^{\text{surf}} r^\lambda \right], \quad (11)$$

$$\phi_\lambda^{(r)}(r > R + L_b) = \sqrt{\frac{4\pi}{2\lambda+1}} \frac{Q_\lambda^{\text{eff}}}{r^{\lambda+1}} \quad (12)$$

with some constants Q_λ . The coefficient Q_λ^{exc} is just the bare 2^λ -pole moment of the exciton polarization:

$$Q_{l+1}^{\text{exc}} = -i\sqrt{(l+1)^2 - m^2} \sqrt{\frac{4\pi}{2l+1}} \int_0^R r^l P^{(r)}(r) r^2 dr, \quad (13)$$

while the contribution of the moment $\lambda = l-1$ turns out to be identically zero when integrated over the dot volume, due to the fact that $P^{(r)}(r)$ vanishes at $r = R$. The background dielectric screening by the polarization charges inside the dot leads to the correction $Q_{l+1}^{\text{exc}} \rightarrow Q_{l+1}^{\text{exc}}/\varepsilon$, taken into account in the expression (11). The coefficient Q_{l+1}^{surf} is determined by the surface polarization charges at the interface $r = R + L_b$ between the media with different dielectric constants ε and $\tilde{\varepsilon}$. The coefficient Q_{l+1}^{eff} is the effective multipole, which determines the field outside the dot. We may relate Q_{l+1}^{surf} and Q_{l+1}^{eff} to Q_{l+1}^{exc} requiring the continuity of $\phi_{l+1}^{(r)}(r)$ and $\varepsilon(r) d\phi_{l+1}^{(r)}(r)/dr$ at $r = R + L_b$, analogously to the procedure of reference [7], which gives

$$Q_{l+1}^{\text{eff}} = \frac{2l+3}{(l+1)\varepsilon + (l+2)\tilde{\varepsilon}} Q_{l+1}^{\text{exc}}. \quad (14)$$

Having calculated the potential, we find the decay rate

$$\begin{aligned} \frac{1}{\tau} &= \frac{\text{Im } \tilde{\varepsilon}}{2\pi\hbar} \int_{|\mathbf{r}| > R+L_b} (\nabla\phi^* \cdot \nabla\phi) d^3\mathbf{r} \\ &= \frac{2l+4}{2l+3} \frac{\text{Im } \tilde{\varepsilon}}{\hbar} \frac{|Q_{l+1}^{\text{eff}}|^2}{(R+L_b)^{2l+3}}. \end{aligned} \quad (15)$$

One may want to average (15) over m , which makes sense since the energy does not depend on the magnetic quantum number m . This is certainly relevant for the case when the dot is pumped electrically, while for the case of excitation by polarized light one should choose the state, corresponding to the given polarization. Such averaging corresponds just to the substitution in (13):

$$\sqrt{(l+1)^2 - m^2} \rightarrow \sqrt{(l+1)(2l/3+1)}, \quad (16)$$

since the radial part of the polarization cannot depend on the quantum number m .

4 The wave functions of the pair: limiting cases

The exciton wave function $\psi(\mathbf{r}_e, \mathbf{r}_h)$ is determined by two interactions: (i) the confinement potential, which we consider to be infinite for $r > R$ and zero at $r < R$, and (ii) the Coulomb attraction of the electron and the hole. The characteristic length scales corresponding to these interactions are R – the quantum dot radius, and a_B – the exciton bulk Bohr radius. Solution of the Schrödinger equation for arbitrary R and a_B is quite a complicated problem (see, *e.g.*, [16,17]), but the situation becomes much simpler in two limiting cases.

If $R \ll a_B$ (strong confinement), Coulomb interaction may be completely neglected and the electron-hole pair wave function will be simply the product of two one-particle wave functions. Each one-particle state is labeled by three quantum numbers: the orbital quantum number $l = 0, 1, \dots$, the magnetic quantum number $m = -l, \dots, l$, and the principal quantum number $n = 1, 2, \dots$ [18]. Denoting this set by a single symbol ν , we may write

$$\psi_{\nu_e, \nu_h}(\mathbf{r}_e, \mathbf{r}_h) = \chi_{\nu_e}(\mathbf{r}_e) \chi_{\nu_h}(\mathbf{r}_h), \quad (17)$$

where the single-particle wave function is given by [18]

$$\chi_{nlm}(\mathbf{r}) \equiv \chi_\nu(\mathbf{r}) = \sqrt{\frac{2}{R^3}} \frac{j_l(\alpha_{ln}r/R)}{j_{l+1}(\alpha_{ln})} Y_{lm}(\theta, \varphi), \quad (18)$$

where $j_l(x)$ is the l -th spherical Bessel function, α_{ln} is its n -th zero ($n = 1, 2, 3, \dots$).

However, to apply the results of the previous section, we have to form the linear combinations corresponding to states with definite total momentum. The new set of quantum numbers is $\{l_e, n_e, l_h, n_h, l, m\}$ and the radial part of the corresponding wave function is expressed in terms of Wigner $3j$ -symbols as

$$\begin{aligned} \psi_{lm}^{(r)}(r) &= \frac{2 \cdot (-1)^{(l_e+l_h+l)/2}}{R^3} \\ &\times \begin{pmatrix} l_e & l_h & l \\ 0 & 0 & 0 \end{pmatrix} \sqrt{\frac{(2l_e+1)(2l_h+1)}{4\pi}} \\ &\times \frac{j_{l_e}(\alpha_{l_e n_e} r/R)}{j_{l_e+1}(\alpha_{l_e n_e})} \frac{j_{l_h}(\alpha_{l_h n_h} r/R)}{j_{l_h+1}(\alpha_{l_h n_h})}. \end{aligned} \quad (19)$$

For $l_e = l_h = l = 0$ this expression is reduced to that obtained in reference [11] to give the dipole moment and the transfer rate

$$Q_1^{\text{eff}} = \frac{3\tilde{\varepsilon} d^{\text{vc}}}{\varepsilon + 2\tilde{\varepsilon}}, \quad \frac{1}{\tau} = \frac{12 \text{Im} \tilde{\varepsilon}}{|\varepsilon + 2\tilde{\varepsilon}|^2} \frac{1}{\hbar} \frac{|d^{\text{vc}}|^2}{(R + L_b)^3}. \quad (20)$$

If $R \gg a_B$ (weak confinement), then the distance between the single-particle levels in the spherical potential well (even for the lighter particle) is much less than the bulk exciton binding energy. In this case the exciton may be considered a rigid particle moving in a spherical well. The relative motion of the electron and the hole and the center-of-mass motion are effectively separated and the wave function is factorized. *E.g.*, for $1s$ -exciton state

$$\psi_{\nu,1s}(\mathbf{r}, \mathbf{r}) = \frac{1}{\sqrt{\pi a_B^3}} \chi_{\nu}(\mathbf{r}). \quad (21)$$

For $l = 0$ we get the result of reference [11]:

$$Q_1^{\text{eff}} = \frac{1}{\pi} \left(\frac{2R}{a_B} \right)^{3/2} \frac{3\tilde{\varepsilon} d^{\text{vc}}}{\varepsilon + 2\tilde{\varepsilon}}, \quad (22)$$

$$\frac{1}{\tau} = \frac{96 \text{Im} \tilde{\varepsilon}}{\pi^2 |\varepsilon + 2\tilde{\varepsilon}|^2} \frac{1}{\hbar} \frac{|d^{\text{vc}}|^2}{a_B^3} \left(\frac{R}{R + L_b} \right)^3. \quad (23)$$

For the numerical estimations we use the parameters, typical for II-VI semiconductors (*e.g.*, CdSe) [19]: $a_B \simeq 50 \text{ \AA}$, $d^{\text{vc}} \simeq 12 \text{ D}$, $\varepsilon \simeq 6$. For the organic part we need to know only the dielectric constant, we take it to be $\tilde{\varepsilon} \simeq 4 + 3i$. This value is not even the most optimistic one, *e.g.* for the PTCDA material, widely used in experiments with organic nanostructures [20], one has $\sqrt{\tilde{\varepsilon}} = n + i\kappa = 2.16 + i1.04$ [21], which gives even larger $\text{Im} \tilde{\varepsilon}$. Having fixed $L_b = 30 \text{ \AA}$, in Figure 1 we plot the transfer times for several strongly confined states, averaged over the magnetic quantum number, as mentioned in the end of Section 3, as a function of the dot radius R . These states are $\{l_e = 0, n_e = 1, l_h = 0, n_h = 1\}$ (dipole transition, solid line), $\{0, 1, 1, 1\}$ (quadrupole transition, long-dashed line), $\{0, 1, 2, 1\}$ (octupole transition, short-dashed line) – the lowest ones, and we take also the $l = 0$ component of $\{1, 1, 1, 1\}$ (the seventh level), the next one after the lowest state, possessing a nonzero dipole moment (dash-dotted line). The upper limit of R is taken to be a_B , since for $R > a_B$ the strong-confinement approximation definitely breaks down. The lower limit of R is different for each state and is taken to be the radius, at which the confinement energy of the state reaches 1 eV, since higher confinement energies are not realistic. We see that for the lowest state the transfer time is quite short – of the order of 10 ps, as it was predicted in reference [11]. The states with larger l have longer times, one may roughly say that every unit of l “costs” about an order of magnitude of τ . This fact, however, might even not spoil the efficiency of the energy transfer since the carrier radiative recombination time will also increase for higher multipole transitions, provided that other relaxation channels are quenched.

We have already mentioned in the Introduction (see Ref. [12]) that the carrier relaxation in quantum dots may be strongly inhibited due to the discreteness of states. In this situation, any material, not necessarily an organic one, with nonzero absorption at the frequency of an *in-traband* transition may affect the intraband relaxation of carriers. The estimation of the relaxation time due to the Förster transfer may be performed along the same lines as for the interband transition, starting from the point that the matrix element of the charge density for the electron (hole) transition from the state $\{l_1, m_1, n_1\}$ to $\{l_2, m_2, n_2\}$ is given by

$$\rho^{\text{exc}}(\mathbf{r}) = \mp e \chi_{l_2 m_2 n_2}^*(\mathbf{r}) \chi_{l_1 m_1 n_1}(\mathbf{r}). \quad (24)$$

This expression should be expanded into spherical harmonics Y_{lm} with $l = |l_1 - l_2|, \dots, l_1 + l_2$, $m = m_1 - m_2$. The intraband transfer rate is given by the same formulas (14, 15) with $l+1$ substituted by l (since there is no differentiation $\partial/\partial z$), but the bare exciton multipole moment, corresponding to the transition rate, averaged over m_1 and summed over m_2 (see the end of the previous section), is given by

$$\begin{aligned} \bar{Q}_l^{\text{exc}} &= 2eR^l \sqrt{\frac{2l_2 + 1}{2l + 1}} \begin{pmatrix} l_1 & l_2 & l \\ 0 & 0 & 0 \end{pmatrix} \\ &\times \int_0^1 dx x^{l+2} \frac{j_{l_1}(\alpha_{l_1 n_1} x)}{j_{l_1+1}(\alpha_{l_1 n_1})} \frac{j_{l_2}(\alpha_{l_2 n_2} x)}{j_{l_2+1}(\alpha_{l_2 n_2})}. \end{aligned} \quad (25)$$

The intraband transitions correspond to the infrared spectral range, where the absorption is usually much weaker than in the visible range. Hence, we set $\tilde{\varepsilon} = 4 + 0.3i$ and evaluate the intraband transition times for the transitions $\{l_1 = 1, n_1 = 1\} \rightarrow \{l_2 = 0, n_2 = 1\}$ (dipole transition – 19 ps), $\{2, 1\} \rightarrow \{1, 1\}$ (dipole transition – 12 ps), $\{2, 1\} \rightarrow \{0, 1\}$ (quadrupole transition – 610 ps) for $R = 30 \text{ \AA}$, $L_b = 30 \text{ \AA}$, shown by the vertical arrows in Figure 1 (in our model the times are the same for electrons and holes). As we see, dipole transitions are much more intensive than higher multipole ones and the times may be relatively short (a few tens of ps). Thus, if other relaxation processes are quenched, the Förster transfer may play some role.

In this connection one may also consider a single-carrier relaxation process, related both to the above considered Förster transfer and to the Auger relaxation, dealt in reference [12]. If one considers an array of quantum dots of characteristic size R , separated by distance r from each other on the wetting layer of thickness L_w (no surrounding organics is assumed), then the following process may occur. Two carriers in the neighbouring dots interact *via* Coulomb interaction (the first nonvanishing multipole component is the dipole-dipole one), then as a result of this interaction, one of the carrier relaxes to a lower state in the dot, while the other is promoted to the wetting layer continuum. This process is adequately described by the Fermi Golden Rule and a simple estimate gives the corresponding time of the order of

$$\tau \simeq \frac{\hbar^3 \varepsilon^2}{m e^4} \frac{r^6}{R^5 L_w}. \quad (26)$$

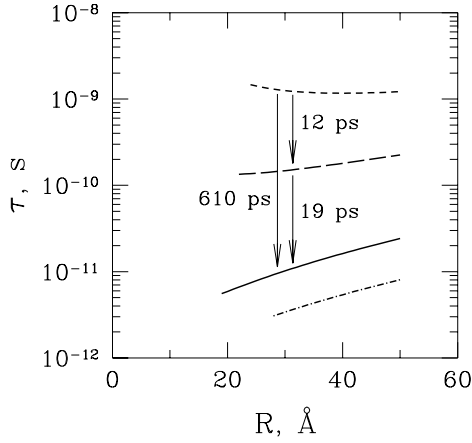


Fig. 1. The Förster transfer time corresponding to the interband transition for II-VI semiconductors in the strong confinement limit from the states $\{0, 1, 0, 1\}$ (solid line), $\{0, 1, 1, 1\}$ (long-dashed line), $\{0, 1, 2, 1\}$ (short-dashed line), $\{1, 1, 1, 1\}$ ($l = 0$, dash-dotted line) versus the dot radius R , $L_b = 30$ Å. The vertical arrows show schematically the intraband transition times (see the text for the details).

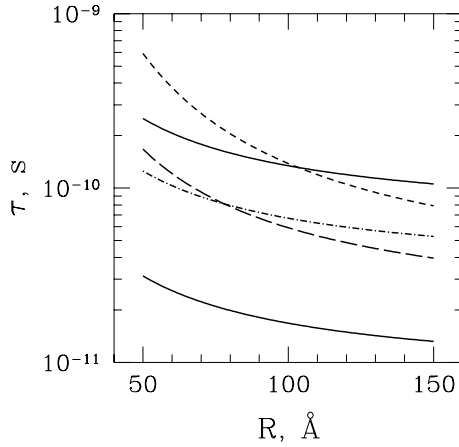


Fig. 2. The Förster transfer time for II-VI semiconductors in the weak confinement limit from the states $\{0, 1\}$ ($1s$ – the lower solid line, $2s$ – the upper solid line), and $1s$ states $\{1, 1\}$ (long-dashed line), $\{2, 1\}$ (short-dashed line), $\{0, 2\}$ (dash-dotted line) versus the dot radius R , $L_b = 30$ Å.

Estimating the first fraction as 10–100 fs, one may obtain numbers of the order of 10–100 ps in a favorable geometry. However, a detailed treatment is beyond the scope of this paper.

Now we return to the energy transfer when the electron-hole pair is annihilated (interband transition), considering the case $R \gg a_B$. In Figure 2 we plot the transfer times for several weakly confined $1s$ -exciton states, the lowest ones – $\{l = 0, n = 1\}$ (the lower solid line), $\{1, 1\}$ (long-dashed line), $\{2, 1\}$ (short-dashed line), $\{0, 2\}$ (dash-dotted line), and the $2s$ -state with $\{l = 0, n = 1\}$ (the upper solid line) as a function of R at fixed $L_b = 30$ Å. The lower limit of R is taken to be a_B , as the upper limit we choose 150 Å, since at larger dot radii the times do not change significantly. From the plots

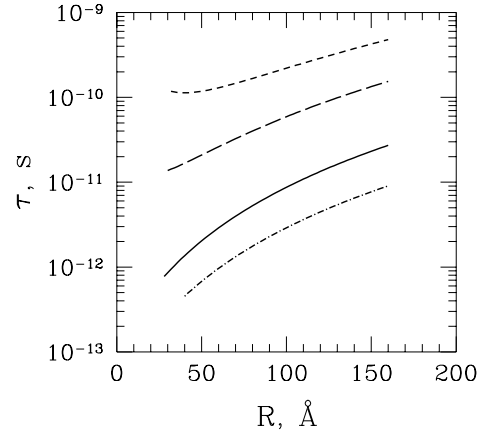


Fig. 3. The Förster transfer time corresponding to the interband transition for III-V semiconductors in the strong confinement limit from the states $\{0, 1, 0, 1\}$ (solid line), $\{0, 1, 1, 1\}$ (long-dashed line), $\{0, 1, 2, 1\}$ (short-dashed line), $\{1, 1, 1, 1\}$ ($l = 0$, dash-dotted line) versus the dot radius R , $L_b = 30$ Å (analogously to Fig. 1).

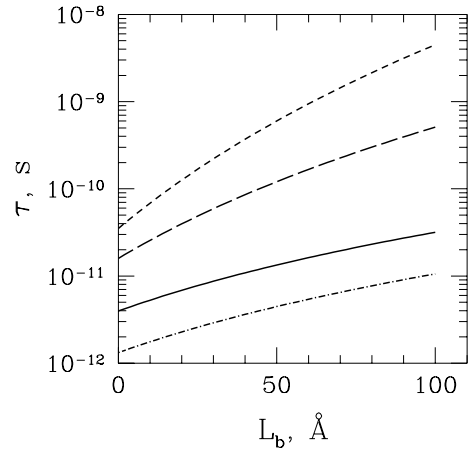


Fig. 4. The same transfer times as in Figure 3 versus the barrier thickness L_b , for $R = 100$ Å.

we see that (i) the transfer from the $2s$ -state is less rapid than that from the $1s$ (by a factor of 8), (ii) the difference between dipole, quadrupole and octupole transitions is not very large (due to the fact that the ratio $R/(R+L_b)$ is not much smaller than 1) and (iii) the dipole transfer from higher excited states with $l = 0$ is slower due to a partial cancellation in the radial integrals.

We have also performed similar transfer rate calculations for parameters typical for III-V materials (*e.g.*, InGaAs): $a_B \simeq 160$ Å, $d^{vc} \simeq 50$ D, $\varepsilon \simeq 9$. Figure 3 shows the transfer times for the same states as in Figure 1 as a function of R for $L_b = 30$ Å for the strong-confinement limit. The times are shorter than those for II-VI semiconductors since the latter have smaller dipole moments d^{vc} . We also plot the transfer time as a function of the barrier thickness L_b for $R = 100$ Å in Figure 4. As one may expect, the higher multipoles, whose electric field decreases more rapidly in space, are more sensitive to the barrier thickness than the lower ones.

5 Variational estimate

To investigate the crossover region between the two limiting cases, that is $R \sim a_B$, we take a simple variational wave function for the lowest excited state:

$$\psi_{a,b}(\mathbf{r}_e, \mathbf{r}_h) = A(a, b_e, b_h) \frac{\chi_0(r_e)}{\sqrt{\chi_0(r_e) + b_e}} \frac{\chi_0(r_h)}{\sqrt{\chi_0(r_h) + b_h}} \times \exp\left(-\frac{|\mathbf{r}_e - \mathbf{r}_h|}{a}\right), \quad (27)$$

where a , b_e , and b_h are positive variational parameters, $A(a, b_e, b_h)$ is the normalization coefficient. The wave function $\chi_0(r)$ is the one given by the equation (18) for $l = m = 0$, $n = 1$:

$$\chi_0(r) = \frac{1}{\sqrt{2\pi R_1}} \frac{\sin(\pi r/R_1)}{r}. \quad (28)$$

The wave function (27) is slightly more general than one proposed long ago by Kayanuma [22]. The latter function did not contain the denominators with the square roots as in the function (27) and depended on the single parameter a . We have chosen the wave function (27) since it reproduces correctly the shape of the *polarization* $\psi(\mathbf{r}, \mathbf{r})$ in both limiting cases: for $R \ll a_B$ both a and b 's become large and one obtains the wave function (17), while for $R \gg a_B$ we have $a \simeq a_B$ (the Wannier exciton ‘‘is formed’’), $b_e, b_h \sim a_B/R^{5/2}$ (the surface corrections to the exciton wave function) and one gets the same polarization as for the wave function (21). The exponential factor is very important since it enhances the probability of finding the electron and hole at the same point, which affects the polarization. The variable ‘‘exciton radius’’ a measures the role of Coulomb correlations between the electron and the hole. The Hamiltonian we consider is given by

$$\hat{H} = \frac{\hat{\mathbf{p}}_e^2}{2m_e} + \frac{\hat{\mathbf{p}}_h^2}{2m_h} + V(r_e) + V(r_h) - \frac{e^2}{\varepsilon_0 |\mathbf{r}_e - \mathbf{r}_h|}, \quad (29)$$

where $V(r)$ is zero for $r < R$ and infinity for $r > R$, ε_0 is the semiconductor background dielectric constant.

To test the wave function (27), we compare the energies obtained from it for different values of R/a_B with those obtained by the exact diagonalization (Ref. [16]) for $m_e = m_h$. The discrepancy is quite small (less than 0.1 Ry). We were not able to repeat the calculation for the value $m_e/m_h = 0.01$ to compare it with the results of reference [16], due to computational problems (for strongly different masses the energy to minimize becomes a very inconvenient function to treat by standard methods). However, having performed the calculations for $m_e/m_h = 0.29$ (the case of CdSe, heavy holes), we see that though the energy is sensitive to the mass ratio, the dipole moment is not (the two corresponding curves in Figure 5 would merge). Thus, we may hope that the wave function (27) reproduces the dipole moment of the dot reasonably well.

Figure 5 shows the transfer times from the lowest state of e-h pair (discontinuous solid line) and the second excited state (discontinuous dashed line) in both limiting

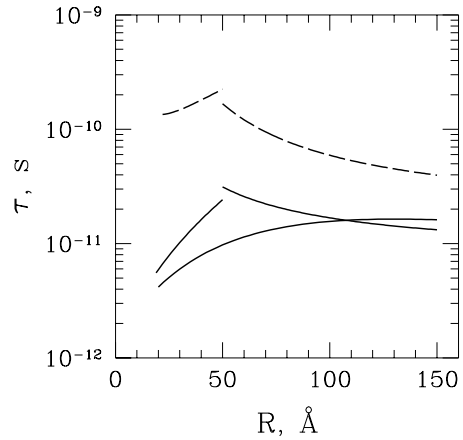


Fig. 5. The transfer times from the lowest state of e-h pair (discontinuous solid line) and the second excited state (discontinuous dashed line) in both limiting cases *versus* the dot radius for the same parameters as in Figures 1, 2. The continuous solid line represents the result of the variational calculation for the lowest state.

cases *versus* the dot radius for the same parameters as in Figures 1, 2. The lowest state is the $\{0, 1, 0, 1\}$ state for the strong confinement and the $\{0, 1\}$ state of 1s-exciton for the weak confinement, while the second excited state is $\{0, 1, 1, 1\}$ and $\{1, 1\}$ respectively. The continuous solid line represents the result of the variational calculation for the lowest state. For $R \sim a_B$ it gives even a more optimistic result. The behaviour of the variational curve at $R > 2a_B$ is somewhat unexpected, however, the detailed inspection of the numbers shows that this curve has a maximum at $R \simeq 3a_B$ and then converges to the limiting curve. We cannot be sure whether this feature is indeed present in the exact solution, or is just due to the poorness of the chosen function. In any case, the discrepancy is not very large (the factor is about 1.3). So, one can say that the estimations using the limiting expressions for the strong and weak confinement describe the situation reasonably well (within a factor of 3).

6 Conclusions

Our calculations for quantum dots show that the Förster energy transfer from the lowest state of the electron-hole pair in the dot to a strong-absorbing organic material is fast enough compared to the carrier recombination time. The transfer times from higher excited states may be longer if the corresponding transition is dipole-forbidden. However, the radiative recombination of the pair in such states should also be suppressed, so we may expect that large part of the quantum dot energy may be transferred to the organic molecules with possible subsequent emission of light. The possibility of pumping quantum dots electrically makes the mechanism, considered here, interesting for applications.

We have also estimated the effect of an organic substance on the carrier intraband relaxation in the case when

the organics has a nonzero absorption coefficient at the frequency, corresponding to the given intraband transition. Unlike intradot Auger processes, such relaxation mechanism does not require more than one carrier inside each dot. Of course, such a process may occur in the presence of any absorbing substance, not necessarily organic.

Partial support from UNESCO through the grant UVO-ROSTE 875.563.9 is acknowledged. V.M.A. is thankful to Scuola Normale Superiore (Pisa, Italy) for hospitality and support. He also acknowledges partial support through Grant 99-03-32178 of the Russian Foundation of Basic Research and Grant 97-1074 "Physics of Nanostructures" of the Russian Ministry of Science and Technology.

References

1. V.M. Agranovich, R. Atanasov, F. Bassani, *Solid State Commun.* **92**, 295 (1994).
2. V.I. Yudson, P. Reineker, V.M. Agranovich, *Phys. Rev. B* **52**, R5543 (1995).
3. A. Engelmann, V.I. Yudson, P. Reineker, *Phys. Rev. B* **57**, 1784 (1998).
4. V.M. Agranovich, G.C. La Rocca, F. Bassani, *JETP Lett.* **66**, 748 (1997).
5. D.M. Basko, G.C. La Rocca, F. Bassani, V.M. Agranovich, *Eur. Phys. J. B* **8**, 353 (1999).
6. V.M. Agranovich, D.M. Basko, G.C. La Rocca, F. Bassani, *J. Phys. Cond. Matter* **10**, 9369 (1998).
7. V.M. Agranovich, M.D. Galanin, *Electronic excitation energy transfer in condensed matter* (North-Holland, 1982).
8. B.O. Dabbousi, M.G. Bawendi, O. Onitsuka, M.F. Rubner, *Appl. Phys. Lett.* **66**, 1316 (1995).
9. D.L. Huffaker, L.A. Graham, D.G. Deppe, *Appl. Phys. Lett.* **72**, 214 (1998).
10. U. Woggon, *Optical Properties of Semiconductor Quantum Dots* (Springer-Verlag, Berlin, 1997).
11. V.M. Agranovich, D.M. Basko, *JETP Lett.* **69**, 250 (1999).
12. R. Ferreira, G. Bastard, *Appl. Phys. Lett.* **74**, 2818 (1999).
13. A similar idea has been used to calculate the energy transfer from an excited dye molecule to the surrounding solution, considering the molecule as a point classical dipole and the solution as a continuous absorbing medium: M.D. Galanin, I.M. Frank, *Zh. Eksp. Teor. Fiz.* **21**, 114 (1951), M.D. Galanin, *Zh. Eksp. Teor. Fiz.* **21**, 126 (1951).
14. L.D. Landau, E.M. Lifshitz, *Electrodynamics of continuous media* (Pergamon Press, 1960).
15. L.D. Landau, E.M. Lifshitz, *The classical theory of fields* (Pergamon Press, 1962).
16. Y.Z. Hu, M. Lindberg, S.W. Koch, *Phys. Rev. B* **42**, 1713 (1990).
17. F. Bassani, R. Buczko, G. Czajkowski, *Nuovo Cimento D* **19**, 1565 (1997).
18. L.D. Landau, E.M. Lifshitz, *Quantum mechanics, non relativistic theory* (Pergamon Press, 1965).
19. R. Cingolani, in *Semiconductors and Semimetals* (Academic Press, 1997), vol. 44, pp. 163–226.
20. S.R. Forrest, *Chem. Rev.* **97**, 1793 (1997).
21. M. Hoffmann (private communication).
22. Y. Kayanuma, *Solid State Commun.* **59**, 405 (1986).